

Gas phase lubrication study with an organic friction modifier

Jennifer Eickworth¹  | Jonas Wagner¹ | Philipp Daum¹ |
Martin Dienwiebel^{1,2}  | Thomas Rühle³

¹Mikrotribologie Centrum, Fraunhofer IWM MikroTribologie Centrum, Freiburg, Germany

²Institute for Applied Materials IAM-ZM, Karlsruhe Institute of Technology, Karlsruhe, Germany

³BASF SE, Ludwigshafen, Germany

Correspondence

Jennifer Eickworth, Fraunhofer IWM MikroTribologie Centrum, Wöhlerstraße 11, Freiburg, Germany.

Email: jennifer.eickworth@iwm.fraunhofer.de

Abstract

Friction modifier additives play a crucial role in controlling friction and wear of lubricated tribological systems. Model experiments in a controllable atmosphere performed by integrating a tribometer into a system of in situ surface analytical methods in vacuum can give insights into the additives functionality. In this work, thin, well-defined layers of an organic friction modifier (OFM) are adsorbed onto an iron oxide surface by means of an effusion cell immediately before measuring friction and wear. The results show that contrary to the assumption that homogeneous layers are formed, this OFM accumulates in droplets on the surface. Droplet number and radius increase with evaporation time. In friction tests, the smallest friction values are found for a low coverage of droplets. For larger droplets, friction increases due to a capillary neck of additive that forms between the sliding surfaces and is dragged along during the friction test.

KEYWORDS

Additives, Friction Modifier, Friction, gas phase lubrication

1 | INTRODUCTION

Friction modifier additives can be roughly divided into organic friction modifiers (OFM), functionalized polymers, soluble organo-molybdenum additives and dispersed nanoparticles.¹ Besides fatty acids, OFMs can comprise carboxylates, alcohols, imides, borates, phosphorus compounds, ionic liquids, amides and amines.² The adsorption and lubrication mechanisms of fatty acids were in the focus of numerous studies during the last century (e.g. References [3–9]) and the friction reduction is often explained using the boundary lubrication model that goes back to Hardy and Doubleday.¹⁰ Later, for some

OFMs a ‘thick film’ lubrication mechanism was also observed that could not be well explained at the time.^{11,12} Moreover, as fatty acids can be corrosive and cause damage, amines and their derivatives are considered a promising alternative. Therefore, recent research on OFMs has triggered new interest and created new opportunities for the friction modifier additives market. The ongoing trend towards low-viscosity oils to reduce liquid friction losses increases the requirements especially for friction modifier additives, as friction must remain low even in the mixed lubrication regime. The adsorption behaviour of amines has been reported in literature (e.g. References [13–18]), but not to such extent as fatty acids. This lack of

This is an open access article under the terms of the [Creative Commons Attribution-NonCommercial-NoDerivs](https://creativecommons.org/licenses/by-nc-nd/4.0/) License, which permits use and distribution in any medium, provided the original work is properly cited, the use is non-commercial and no modifications or adaptations are made.

© 2022 The Authors. *Lubrication Science* published by John Wiley & Sons Ltd.

knowledge and more stringent environmental guidelines encourage a better understanding of the adsorption and mode of action of amine-based friction modifiers.

During friction tests, complex reactions can occur in boundary lubrication between the contacting asperities and the additives. It can be very difficult to understand these mechanisms in an oil-lubricated situation because of the interaction of base oil with the additives. Hence, performing model experiments in a controllable atmosphere is insightful.¹⁹ This can be achieved by integrating a tribometer into a system of in situ surface analytical methods in vacuum, for instance comprising a X-ray photoelectron spectrometer (XPS), an Auger electron spectrometer (AES) or a secondary ion mass spectrometer, allowing the chemical composition of surfaces to be investigated before and after tribological experiments without atmospheric influence. Using an effusion cell or an electron beam evaporator allows the deposition of molecularly thin lubricant or additive layers on a defined surface. Variable leak valves can also be used to change the partial pressure of a specific background gas in which the friction experiments take place. J. M. Martin's group developed a so-called 'Environmental Controlled Analytical Tribometer (ECAT)' in the 1990s. This consists of a UHV chamber for tribological experiments, an XPS/AES system and a UHV preparation chamber (see e.g. in References [19] and [20]). Similarly, in subsequent works an home-built UHV microtribometer coupled to the existing XPS system was developed.²¹ In addition, an electron beam evaporator and an effusion cell were installed for the deposition of organic layers.

Extensive work has been carried out over the last 30 years on the frictional properties of various model substances relevant to technical lubricants. The measurements were realised with the ECAT and often follow a similar pattern. A leak valve is used to control the partial pressure of the substances under investigation. The rubbing experiments are then carried out at controlled partial pressures, with a reference measurement in the liquid substance. XPS surface analysis is used to collect and evaluate additional information about the reaction mechanisms taking place. To date, studies with triethyl phosphite,^{22,23} triethyl borate,²⁴ phosphororganous compounds²⁵ and hexanthiol¹⁹ have been conducted. Another study by Rana and Tysoe investigated the influence of triethylphosphates and -phosphites on the frictional behaviour of oxidised Fe₃O₄ iron.²⁶

The correlation of measurements in vacuum and in liquid, that is, the state of a technical lubricated contact, could be shown by Martin et al.²⁷ Microscopic images of a friction track after experiments in a controlled ethylphosphate atmosphere in the tribo-chamber (10 Pa) and in liquid show a similar morphology. Therefore, it can be

assumed that the friction mechanisms occurring in liquid-phase lubrication are well represented.

To our knowledge, studies so far have used model substances which do not have the same functional groups as common friction modifiers or anti-wear additives. Although, this allows adsorption and reaction mechanisms to be elucidated, the systems are also greatly simplified and the influence of molecular structures, chain lengths and resulting interactions between the additive molecules cannot be taken into account. In the present study, the aim is to apply layers of a commercial friction modifier of different thickness and then to investigate the influence of the layer thickness on film morphology and friction behaviour.

2 | MATERIALS

A commercially available, nitrogen-containing, OFM was used. It is an organic compound the chemistry and relevant physical properties of which are broadly described in Reference [28]. The head group can be a propyl, ester or alcohol group.

Plate-shaped samples are made of 99.5% pure iron(III) oxide (FE000414, GoodFellow GmbH, Hamburg, Germany). In order to achieve a reproducible surface quality, the plates are pre-processed on a semi-automatic grinding and polishing machine (Buehler PowerPro 4000, Buehler ITW Test & Measurement GmbH, Esslingen a. N., Germany). For the grinding steps, a SiC paper (WS flex 18 C SK, Hermes Schleifmittel GmbH, Hamburg, Germany), with grit sizes of 1200 (3 min, 35 N, rpm plate: 200), 2400 (3 min, 50 N, rpm plate: 200) and 4000 (2 × 2 min, 50 N, rpm plate: 150) is used. The coolant used during grinding is water. This is followed by two polishing steps with a polishing cloth (Microcloth SPT069 - PT Seda S, Cloeren Technology GmbH, Wegberg, Germany) together with 3 and 1 μm monocrystalline diamond paste (DPA-M006 and DPA-M007, Cloeren Technology GmbH, Wegberg, Germany) (3 min each, 50 N, revolutions/min plate: 150). The coolant used during the polishing steps is ethanol-based (Lubricant Brown or Lubricant Blue, Cloeren Technology GmbH, Wegberg, Germany). The speed of the machine head is 150 rpm. Between each grinding and polishing step, the specimens and their holder are cleaned under running water to remove grinding particles. After separation of the specimens from the holder, they are cleaned in an ultrasonic bath for 5 min each in acetone and then isopropanol. The polished plates have an average roughness of $R_A = 0.84 \pm 0.33 \mu\text{m}$. A diamond ball segment (Synton-MDP AG, Nidau, Schweiz) with a radius of 5.81 mm is used as a counter body.

3 | METHODS

To determine the coefficient of friction without the influence of the environment and the base oil, a tribometer in vacuum is used. The ball-on-plate tribometer used in this work is a home-made design which is described in more detail in a publication by Marchetto et al.²¹ The sample (an iron plate) sits on a sample plate, which in turn sits on a piezo actuator (stage). The actuator allows a highly precise movement of the specimen in the x -, y - and z - directions (100 μm each). Control of the tribometer and data acquisition is carried out with LabView. The counter body is attached to a cantilever using superglue (UHU superglue, UHU GmbH, Brühl, Germany). In the friction test, the cantilever is deflected in the z -direction (normal force F_N) and in the y -direction (F_T), so that the coefficient of friction can be identified from the ratio. The amount of deflection is determined with a laser interferometer. Two mirrors are placed perpendicular to one another on the tip of the cantilever, directly above the counter body. Two incident laser beams (z - and y - direction) are reflected by the mirrors so that the deflection can be determined. Figure 1 shows the setup of the tribometer.

The tribometer is connected to a vacuum transfer system so that the samples can be characterised before and after the friction tests using XPS. The entire measurement setup is shown in Figure 2.

An effusion cell (Low Temperature Effusion Cell NTEZ, Dr. Eberl MBE-Komponenten GmbH, Weil der Stadt, Germany) is used to evaporate samples (here a friction modifier additive) for gas phase deposition. The effusion cell is integrated into the vacuum measurement system shown in Figure 2, so that the sample (i.e. the iron plate) can be cleaned in the XPS chamber by sputtering off the upper nanometres and then transferred into the effusion chamber without contact to atmosphere. Approximately 10 μg of the additive to be evaporated is brought into the effusion cell in a quartz test tube. The test tube is then heated electrically via a resistance heating wire by adjusting the voltage U and the current I . A mass spectrometer (PrismaPlus QMG 220, Pfeiffer Vakuum GmbH, Aßlar, Germany) is used to monitor the vapour pressure during the evaporation.

For chemical composition analysis, an XPS, Versa Probe II (Physical Electronics, Inc. [PHI], Chanhassen MN, USA) is used. The spectrometer, operating in vacuum $<10^{-6}$ mbar, is equipped with a monochromatic Al- $K\alpha$ X-ray source (1486.6 eV) that achieves a minimum beam radius of 20 μm . The surface composition is measured with an XPS typical information depth <5 nm. For overview spectra (0–1400 eV), pass energies of 187 eV are set in the hemisphere analyser. In order to achieve a better resolution in the detail spectra of the individual

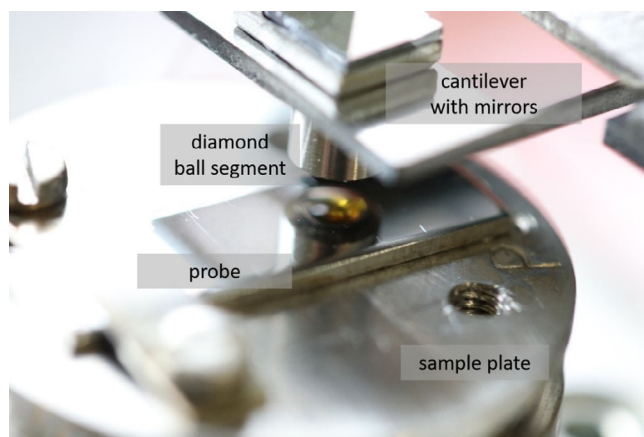


FIGURE 1 Setup of the UHV tribometer with an iron plate probe (mounted on sample plate) and a diamond ball segment as counter body (mounted on a cantilever with a mirror construction for measurements of the normal and transversal forces by interferometry).

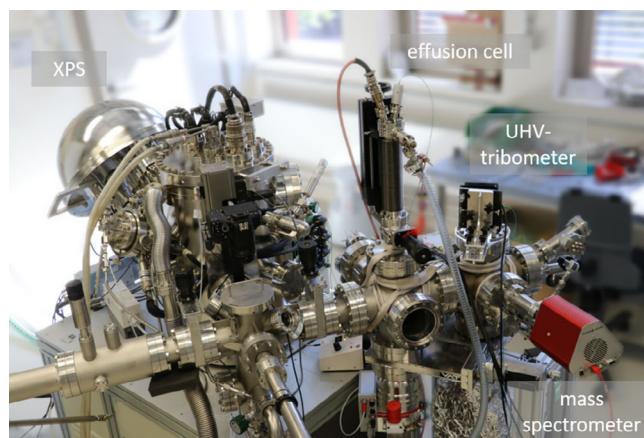


FIGURE 2 Measurement set-up at MikroTribologie Centrum μTC Karlsruhe with photoelectron spectrometer (XPS), effusion cell, tribometer and mass spectrometer

emission lines, the pass energy is lowered to 23 eV. The composition in atomic percent at.-% is calculated from the area integrals below the emission lines.

The steps of the experimental routine are described in more detail below.

After the samples have been introduced into the vacuum measurement system, they are cleaned of organic impurities by sputter cleaning in the XPS, which removes a maximum of 3 nm of the surface. For this purpose, the surface is sputtered in (5×5) mm² squares with 2 kV and 2000 nA each. The sputter rate with this setting is calibrated to SiO₂ and amounts to approx. 2.5 nm/min. An overview spectrum is measured to confirm the cleaning step and to determine the composition of the initial surface.

For gas phase evaporation, the cleaned samples are transferred into the effusion chamber and kept outside the deposition radius of the effusion cell. Later, when the actual evaporation starts, the sample is positioned centrally below the effusion cell. The cell's temperature is controlled via resistance heating and the temperature is raised stepwise by increasing the voltage to 4 V in steps of 0.5 V/min. The current is readjusted accordingly. Through thermogravimetric analysis (TGA) of the friction modifier, it is known that the additive evaporates in three stages (supplementary information). At 134.9°C, 18.5% of the additive evaporates. The largest amount, 77.9%, evaporates at 217.4°C while at 353.3°C a residue of 3.6% passes into the gas phase. Since the TGA measurement was performed at 1 Pa and the effusion cell operates in four to five orders of magnitude better vacuum, it can be assumed that evaporation already starts at lower temperatures. Figure 3 therefore shows a mass spectrum of the friction modifier during evaporation at about 235°C.

Beginning at a temperature of about 235°C, the intensity of mass number 114 increases. A temperature increase beyond that does not lead to an additional increase of the intensities, so that it can be assumed that at this temperature the entire additive is evaporated (see also the TGA-measurement in the supplementary information). Since all components of the additive are deposited onto the iron plate, this mass number is used as an indicator. During evaporation, for the sake of clarity, only the partial pressures (p_i) of the individual components

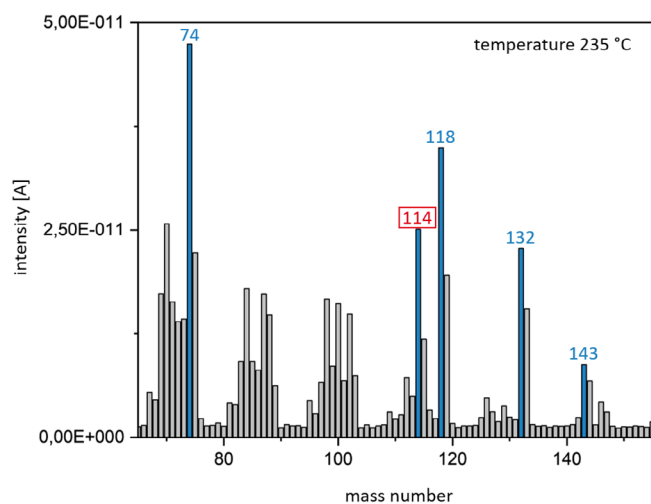


FIGURE 3 Intensities versus mass numbers during evaporation of the friction modifier at approx. 235°C. The blue bars show the mass numbers 74, 114, 118, 132 and 143, which are characteristic for the friction modifier, while the grey bars represent background and other non-specific mass numbers. Mass number 114 (marked in red) represents the last evaporation stage

(p_{74} , p_{114} , p_{118} , p_{132} and p_{143}) are monitored over time. Once the partial pressure of mass number 114 reaches the maximum, the sample is positioned at a distance of 10.6 cm centrally below the effusion cell. In order to determine the influence of film thickness on the frictional behaviour, experiments are performed with a duration of 5 s, 30 s, 2 min, 4 min and 6 min. After evaporation, the coated samples are transferred to the tribo-chamber.

In the tribo-chamber, the coated specimen is positioned on the microtribometer stage. The counterbody used is a diamond ball segment with a radius of 5.81 mm. The normal force is set to 5 mN (average Hertzian pressure of 70 MPa), which is the lowest load possible with the instrument. The low Hertzian pressure is to ensure measuring without generating excessive wear. The sliding distance is set to 100 μm and speed to 50 $\mu\text{m/s}$. Each of the 222 cycles consists of a 100 μm long outward and return path.

After the friction tests, the sample is transferred from the tribo-chamber back into the XPS chamber. Here, both an overview or wide-scan spectrum (0–1400 eV, pass energy 187 eV) and detail spectra of the emission lines of oxygen O1s, carbon C1s, nitrogen N1s and iron Fe2p are recorded. The measurements are performed in the area of the plate that appears matte in Figure 4. The area with the friction marks can be clearly seen in the centre.

Following surface analysis, the surface is sputtered again in the area of the friction marks at the same setting as the initial sputter cleaning (2 kV, 2000 nA, $5 \times 5 \text{ mm}^2$). For the samples, which were coated for 5 s and for 30 s, this step is omitted.

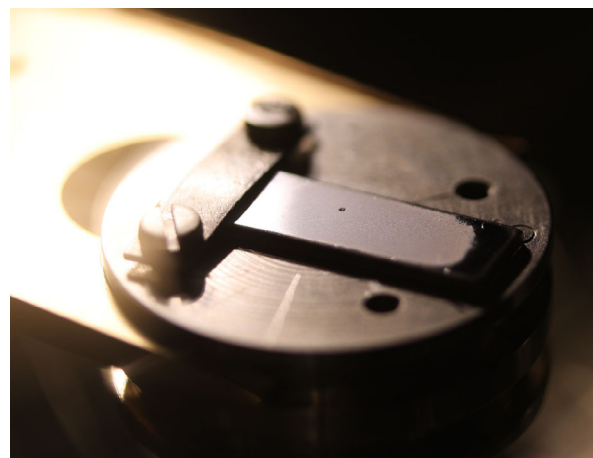


FIGURE 4 Sample carrier with iron plate after 4 min of gas deposition and a friction test. The dull area in the centre of the plate is covered with the friction modifier; the area with the friction marks are clearly visible in the centre.

Afterwards the samples are transferred to the tribochamber again to measure the friction force after sputtering. These subsequent friction tests are carried out with the same parameters mentioned above.

Finally, light microscope images and 3D topography images are taken of the surfaces and the friction tracks using a confocal microscope. These measurements are made outside the vacuum of the measurement system so that the surfaces are exposed to atmosphere.

4 | RESULTS

4.1 | Gas phase deposition

Additives were deposited with different the deposition times of 5 s, 30 s, 2 min, 4 min and 6 min. The accompanying analysis with the mass spectrometer, as well as the prevailing pressures and temperatures is shown in the supplementary information.

The chemical composition of the iron plates after gas phase deposition was examined via XPS. Table 1 lists the results for the tests. After sputter cleaning (process step 1), the iron content (Fe) on the surface averages 40.7 at.%. Oxygen is present at an average of 57.1 at.%. Sputter cleaning can reduce the carbon content to an average of 2.2 at.%. The carbon content after gas deposition can thus be mostly attributed to the gas-deposited additive. After evaporation, the carbon content increases to 56.1 at.% (5 s), 73.7 at.% (30 S), 68.5 at.% (2 min), 65.5 at.% (4 min) and 65.7 at.% (6 min). The element characteristic of friction modifiers, nitrogen (N), is now present at the surface at 3.2 at.% (5 s), 2.9 at.% (30 s), 2.9 at.% (2 min), 4.5 at.%

(4 min), and 7.7 at.% (6 min). The nitrogen content increases with longer deposition time, with the very short gas deposition time of 5 s being an exception here with 3.2 at.%. The iron and oxygen contents decrease to an average of 6.4 and 23.4 at.%, respectively, as a result of the deposition with friction modifier.

Figure 5 shows the emission lines of oxygen O1s, carbon C1s, nitrogen N1s and iron Fe2p for the iron plate's surface after the deposition for 2 min (red lines). Furthermore, the spectra of the initial surface (blue lines) and pure friction modifier (grey lines) are shown. The spectra of the substrate and friction modifier can be found in detail and with labels for the individual lines in the supplementary information—the raw data is provided in.²⁹ The initial surface consists of iron oxides and a small amount of metallic iron. Either the metallic iron can be detected below the thin oxide layer, or the oxide layer is not continuous and metallic iron is exposed at some places. The friction modifier coating consists of various organic compounds consisting of carbon, oxygen and nitrogen, so that in addition to ether groups (C–O), carbonyls (C=O) and various amino compounds (NC₃, HNC₂, H₃N) are also detected. After gas phase deposition of the friction modifier on the initial surface, the emission lines for oxygen, carbon and nitrogen shift slightly towards higher binding energies. There is no change in the chemical composition of the friction modifier. The emission lines of oxygen and iron (iron oxides) resulting from the substrate are still detectable after gas deposition, but the intensity decreases significantly.

After the surface analysis of the coated plates, a 25 mm² area is sputtered around the pre-existing friction marks (ablation <3 nm, calibrated to SiO₂). Further friction tests are subsequently carried out on this portion of the surface (see the following section). The chemical composition in the sputter area can be taken from Table 2. The test with an evaporation time of 6 min was carried out with a new iron plate, so that the initial and the sputtered surfaces are compared.

After sputtering the coated surface, iron is no longer detected. The oxygen content is also reduced to 12.8 at.% on average. Both the carbon and nitrogen contents increase to an average of 81.9 and 5.3 at.%, respectively. The corresponding spectra for the sample after a sputtering time of 2 min are shown in Figure 6. We notice that after sputtering, the chemical composition of the friction modifier does not change.

Figure 7 shows sections from microscopy images taken with the confocal microscope of the iron plate surfaces coated with friction modifier. The initial surface shows some fine grinding marks and some isolated surface defects or impurities (black spots). After 5 s of deposition, the grinding grooves of the initial surface are still

TABLE 1 Chemical composition of the iron plate surface after sputter cleaning (initial) and after evaporation (steamed) for the 5 s, 30 s, 2 min, 4 min and 6 min experiments

		Fe	O	C	N
		[at.-%]			
5 s	Initial	52.8	43.7	3.5	0
	After deposition	9.1	31.6	56.1	3.2
30 s	Initial	53.5	44.3	2.1	0
	After deposition	5.2	18.2	73.7	2.9
2 min	Initial	30.7	68.4	0.9	0
	After deposition	5.2	23.3	68.5	2.9
4 min	Initial	33.6	64.1	2.3	0
	After deposition	6.3	23.6	65.5	4.5
6 min	Initial	32.7	64.9	2.4	0
	After deposition	6.4	20.3	65.7	7.7

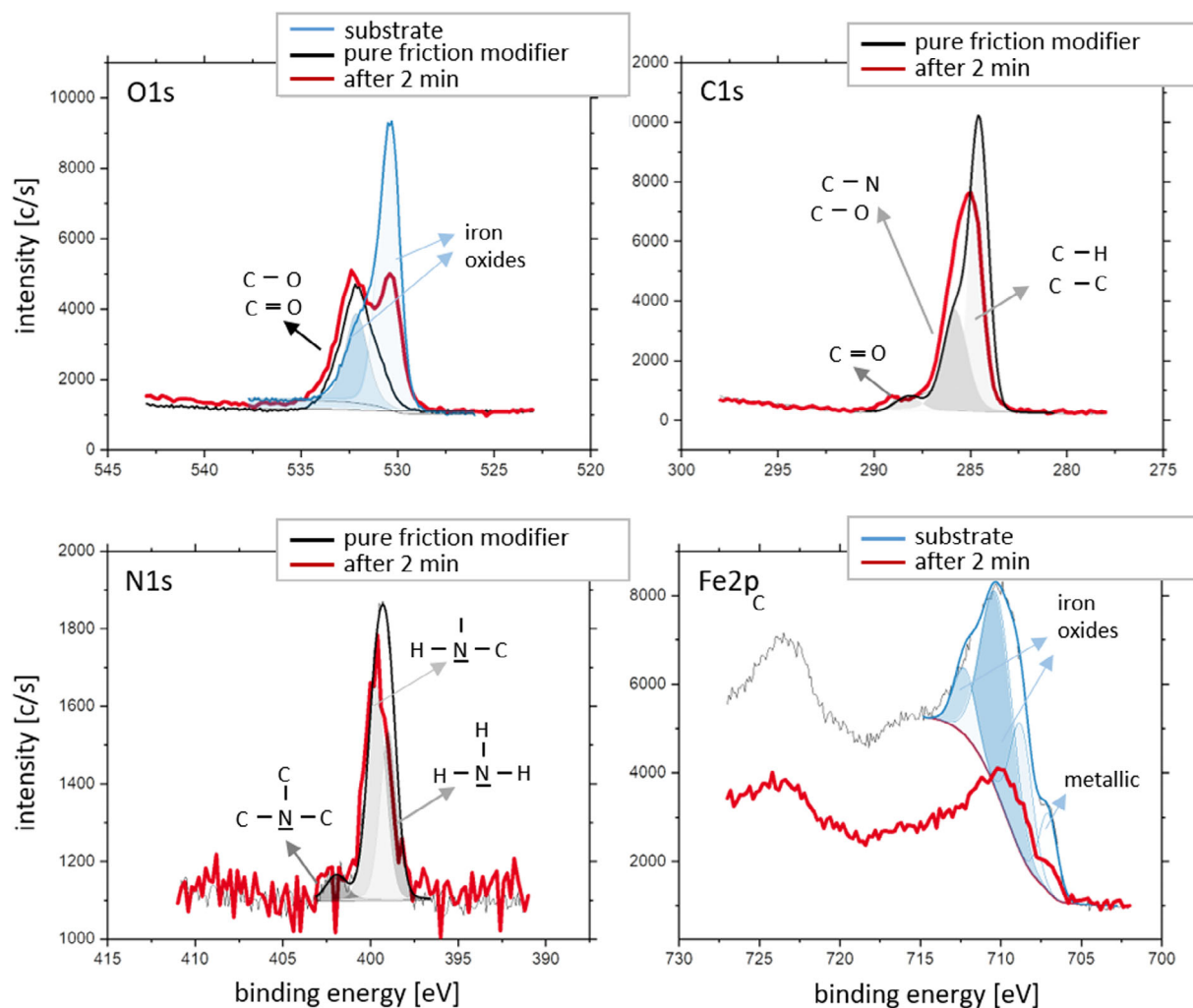


FIGURE 5 XPS high resolution spectra of the iron plate after 2 min evaporation with friction modifier (red lines) as well as the lines for the initial surface (blue lines) and the pure friction modifier friction modifier (grey lines), indication of the emission lines of oxygen O1s, carbon C1s, nitrogen N1s and iron Fe2p

TABLE 2 Chemical composition of the iron plate surface after deposition and after sputtering (sputtered) for the 2, 4 and 6 min experiments

		Fe	O	C	N
		[at.-%]			
2 min	After deposition	5.2	23.3	68.5	2.9
	Sputtered	0	12.7	82.4	4.9
4 min	After deposition	6.3	23.6	65.5	4.5
	Sputtered	0	12.7	81.5	5.9
6 min – 2	Initial	28.5	70.6	0.9	0
	Sputtered	0	13.1	81.8	5.1

visible and areas with an accumulation of small islands with a relatively uniform diameter of values $<0.05 \mu\text{m}$ appear. Since the larger black features are most likely the

same defects or impurities that were observed for the initial surface, it is feasible that the islands appear due to the adsorption of additive. After 30 s of deposition, the surface coverage with homogeneously distributed islands is almost complete. After 2 min, the diameter (approx. $1 \mu\text{m}$) and height of islands have grown further. A Matlab code was employed for circle detection and to evaluate the droplet size and number. Since the island size corresponds approximately with the size of a pixel, they cannot be automatically detected. However, the algorithm recognises that these are modified areas which account for an area share of 11%. After 4 min of evaporation, 27% of the surface is covered with droplets which equals 79 droplets per $(100 \times 100) \mu\text{m}^2$. The mean radius has further grown, presumably due to Ostwald ripening, to $3.2 \pm 0.68 \mu\text{m}$. The circle detection image and the corresponding histogram are given in the supplementary information. For the longest evaporation time (6 min),

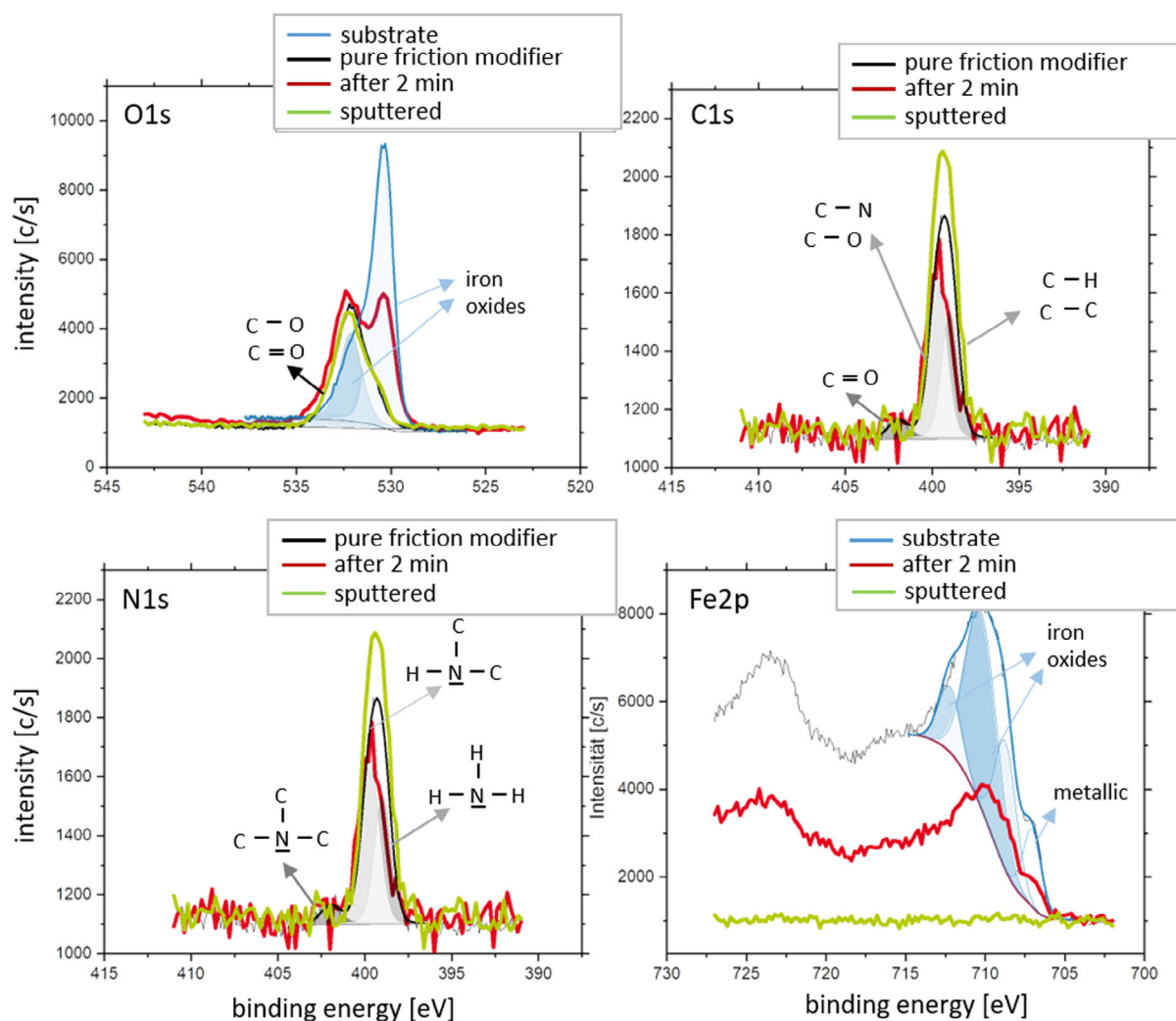


FIGURE 6 XPS high resolution spectra of the iron plate coated for 2 min (red lines) and the subsequent sputtering step (green line) as well as the lines for the initial surface (blue lines) and the pure friction modifier (grey lines), indicating the emission lines of oxygen O1s, carbon C1s, nitrogen N1s and iron Fe2p.

2967 droplets are detected on the surface, covering 26% of its area at a droplet density of 97 droplets per $(100 \times 100) \mu\text{m}^2$. The droplets have an average radius of $3.5 \pm 0.79 \mu\text{m}$. The images with the circle detection and the corresponding histograms are given in the supplementary information.

4.2 | Friction

For comparison, the dry friction tests (shown in Figure 8) will first be described. The chemical composition of the surface for dry friction tests 1 and 2 corresponding to the average values of the initial surfaces are described in Table 1. In addition, small amounts of nitrogen and potassium were found on the surface (0.9 at.%), which

can be attributed to contamination from the previous tests in the effusion chamber.

For each cycle, the friction force is recorded in forward and reverse sliding direction resulting in a lateral force loop. The mean value of the friction force F_R is divided by the mean normal force F_N of the respective friction test, so that the coefficient of friction COF is determined as the quotient. Each friction value determined in this way forms a data point. Since the tests are performed in a reversible motion, the piezo element accelerates or decelerates near the reversal points. In order to consider only intervals of constant velocity, all data points of the friction loops that are at a distance $<3 \mu\text{m}$ from the reversal points are not included in the mean value calculation. The complete raw data of the individual friction tracks is given in Reference [29]. The

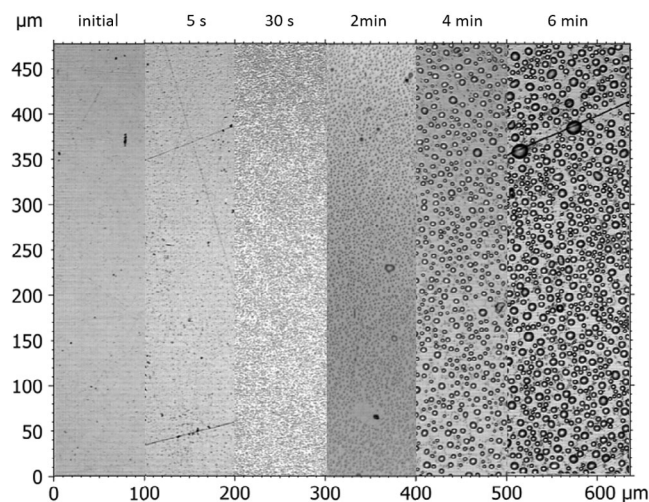


FIGURE 7 Grey images of the iron plate surfaces coated with friction modifier after 5 s, 30 s, 2 min, 4 min and 6 min and the initial surface without gas deposition.

evaluation scheme is attached in the supplementary information on the basis of an example measurement.

The summarised results of the dry friction tests are plotted in Figure 8. During the dry friction test, the average normal force is 5.2 ± 0.7 mN. The average COF value was 0.19 ± 0.09 at the beginning of the test and continuously increased to 0.29 ± 0.22 by the end of the test. A trend cannot be identified with respect to the order of the individual friction tracks. With the exception of friction track 3, the friction values stabilise between 100 and 150 cycles. For the second dry friction experiment, the normal force of 5.7 ± 0.5 mN is around 0.5 mN higher than for the first dry friction experiment. At the start of the test, the average coefficient of friction is 0.13 ± 0.02 . Over the first 25 cycles, the coefficient of friction then decreases (run-in) and then remains constant until approx. 120 cycles. After 120 cycles, the coefficient of friction increases significantly for all individual friction

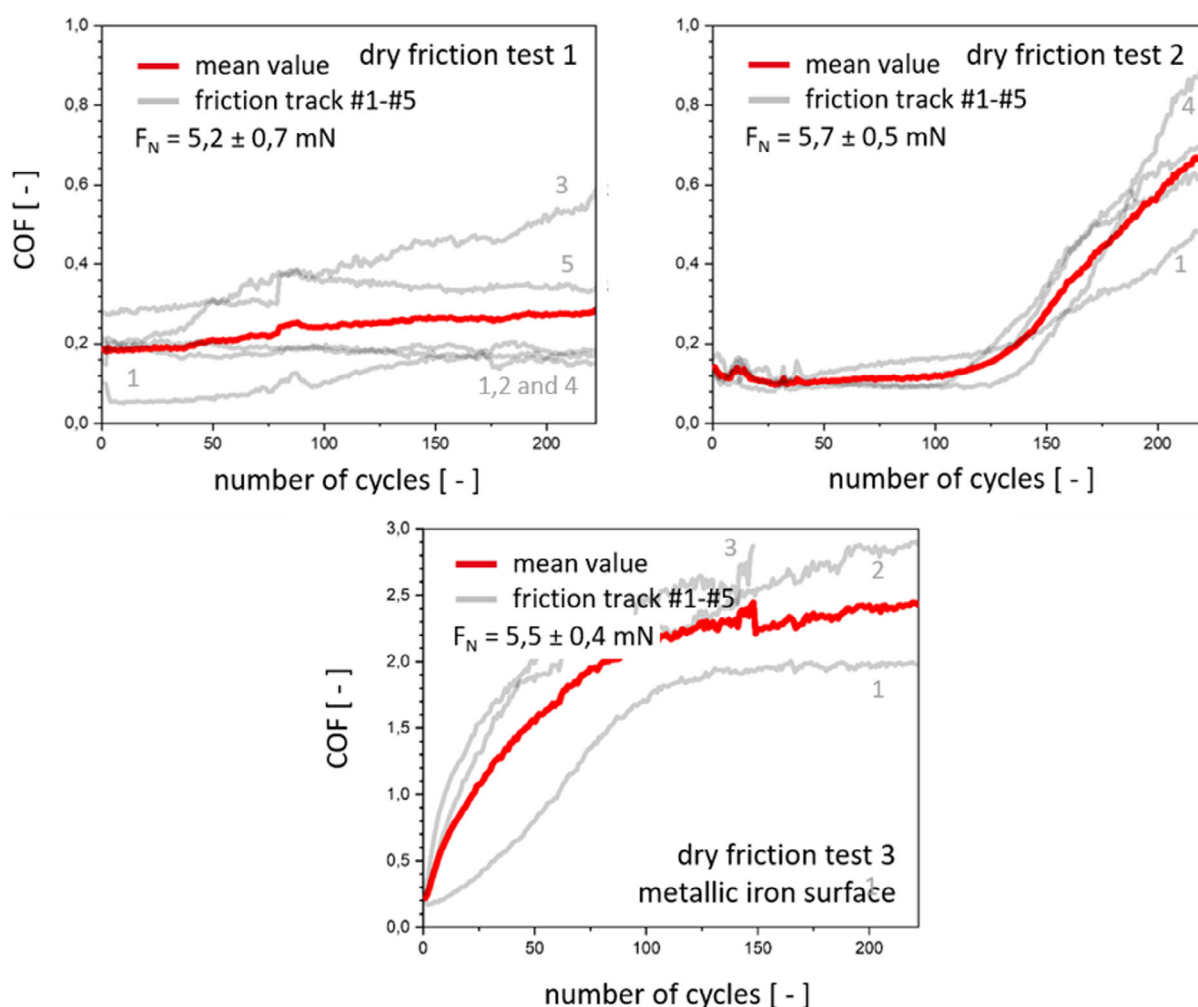


FIGURE 8 Coefficient of friction versus number of cycles for the UHV tribometer tests for dry friction, counterbody diamond ball, nominal normal force $F_N = 5$ mN (corresponds to a mean Hertzian pressure of 70 MPa), number of cycles $N = 222$, velocity $v = 50$ $\mu\text{m/s}$ (reversing), grey curves: single friction tracks (partially numbered), red curves: same mean value of the single friction tracks.

tracks reaching 0.51 ± 0.02 on average at the end. The slope increases with ascending order of the individual friction tracks.

The dry friction track 3 is measured on a surface with an increased proportion of metallic iron. For this purpose, the initial surface (iron oxide with organic impurities) is removed by sputtering off 30 nm so that 72.6 at.% iron and 26.8 at.% oxygen are still present on the surface. The evaluation of the Fe2p line shows that it is 57.57 at.% metallic and 42.43 at.% oxidic iron (supplementary information). For the dry friction test 3, the normal force is 5.5 ± 0.4 mN. The progression of the friction coefficients is similar for all friction tracks. At the beginning, it averages 0.21 ± 0.001 and then increases to 2.4 ± 0.4 with a depressive trend. Here the friction jumps steeply at about 150 cycles and the friction coefficient rises into the triple-digit range. Since the cantilever spring does not permit such high forces, this is presumably a measurement error. Therefore, the corresponding data is excluded from the mean value calculation from 150 cycles onwards.

The friction tests on the iron plates coated with friction modifier are shown in Figure 9. For the shortest deposition time of 5 s, the friction coefficient is constant at a level of 0.06 to 0.05. Track 1 shows the highest friction coefficient, while the friction coefficients of tracks 2 and 3 are at a similar but lower level. For 30 s evaporation duration, the average friction value at the beginning is 0.04 ± 0.01 . After approx. 50 cycles, the friction value for tracks 1 and 2 starts to increase. The coefficient of friction of track 3 remains constant. The average coefficient of friction at the end of the test is 0.07 ± 0.02 . For the deposition duration of 2 min, the average coefficient decreases from 0.1 ± 0.02 to 0.07 ± 0.01 over the first 25 cycles. After 25 cycles, the friction value increases again. For tracks 1 and 3, the coefficient of friction reaches a maximum between 100 and 150 cycles before decreasing again. The coefficient of friction track 2 first does not increase as much then decreases again after 75 cycles and finally remains constant from cycle 100. At the end of the test, the average coefficient of friction is 0.11 ± 0.04 . The average normal force for the test is 5.4 ± 0.3 mN. For the friction tests on the iron plate coated for 4 min, the normal force is 5.4 ± 0.4 mN. The friction coefficient decreases from 0.16 ± 0.02 to 0.07 ± 0.01 on the first 50 cycles and then increases to 0.09 ± 0.001 by the end of the experiment. Friction track 3 exhibits a non-plausible jump at cycle 170 and is therefore no longer taken into account for the mean value calculation. After an evaporation duration of 6 min, the friction value decreases continuously from an initial average of 0.09 ± 0.02 to 0.06 ± 0.02 . Track 1 shows the

highest friction value and the most unstable course compared with tracks 2 and 3. The normal force for this test was 5.7 ± 0.5 mN.

Figure 10 shows the friction coefficient curves for the tests on the coated and subsequently sputtered surfaces. The friction tests are carried out on the sputtered area. The tests on the 2 min deposited plates are carried out with a normal force of 5.5 ± 0.5 mN. The coefficient of friction decreases from 0.17 ± 0.02 on the first 25 cycles to 0.08 ± 0.01 and then remains stable, averaging 0.09 ± 0.03 at the end. In the sputtered area after 4 min of deposition, the coefficient of friction decreases from 0.13 ± 0.01 to 0.07 ± 0.00 within the first 50 cycles and then remains stable. No run-in is observed for the test after 6 min deposition time. The coefficient of friction decreases continuously from 0.11 ± 0.02 to 0.07 ± 0.02 . The normal force was 5.8 ± 0.7 mN.

Following the friction tests on the coated specimens, the friction marks are clearly visible. They are located in the centre of an approximately circular recess in the otherwise droplet-covered plate surface. This effect is most clearly seen on the sample that was coated for 6 min (see Figure 11). A large elongated droplet spreads out over three friction tracks. The topography image depicted in Figure 11, shows that the friction tracks represent wear scars up to $1 \mu\text{m}$. The same effect can be observed for the other evaporation durations.

5 | DISCUSSION

The gas phase lubrication experiments aimed at applying layers of a commercial friction modifier of different thickness in order to investigate the influence of the layer thickness on the friction behaviour. In the first step, iron plates with a native oxide layer were coated with friction modifier using an effusion cell. The gas phase deposition was successfully carried out for deposition durations of 5 s, 30 s, 2 min, 4 min and 6 min. Surface chemical analysis shows that gas phase deposition decreases the iron content from 30.7% (initial) to 5.2–6.4 at.%. By contrast, the content of nitrogen, which can be regarded as a marker for the friction modifier, increases to 3.2 at.% (5 s), 2.9 at.% (30 s and 2 min), 4.5 at.% (4 min) and 7.7 at.% (6 min). Ergo, with increasing deposition durations, the content of nitrogen also increased. The XPS spectra show that the chemical composition of the additive does not change as a result of evaporation and condensation on the surface (see Figure 5).

Ex situ images of the coated surfaces taken with a confocal microscope show that the additive adsorbs with a droplet-shaped morphology using vapour deposition

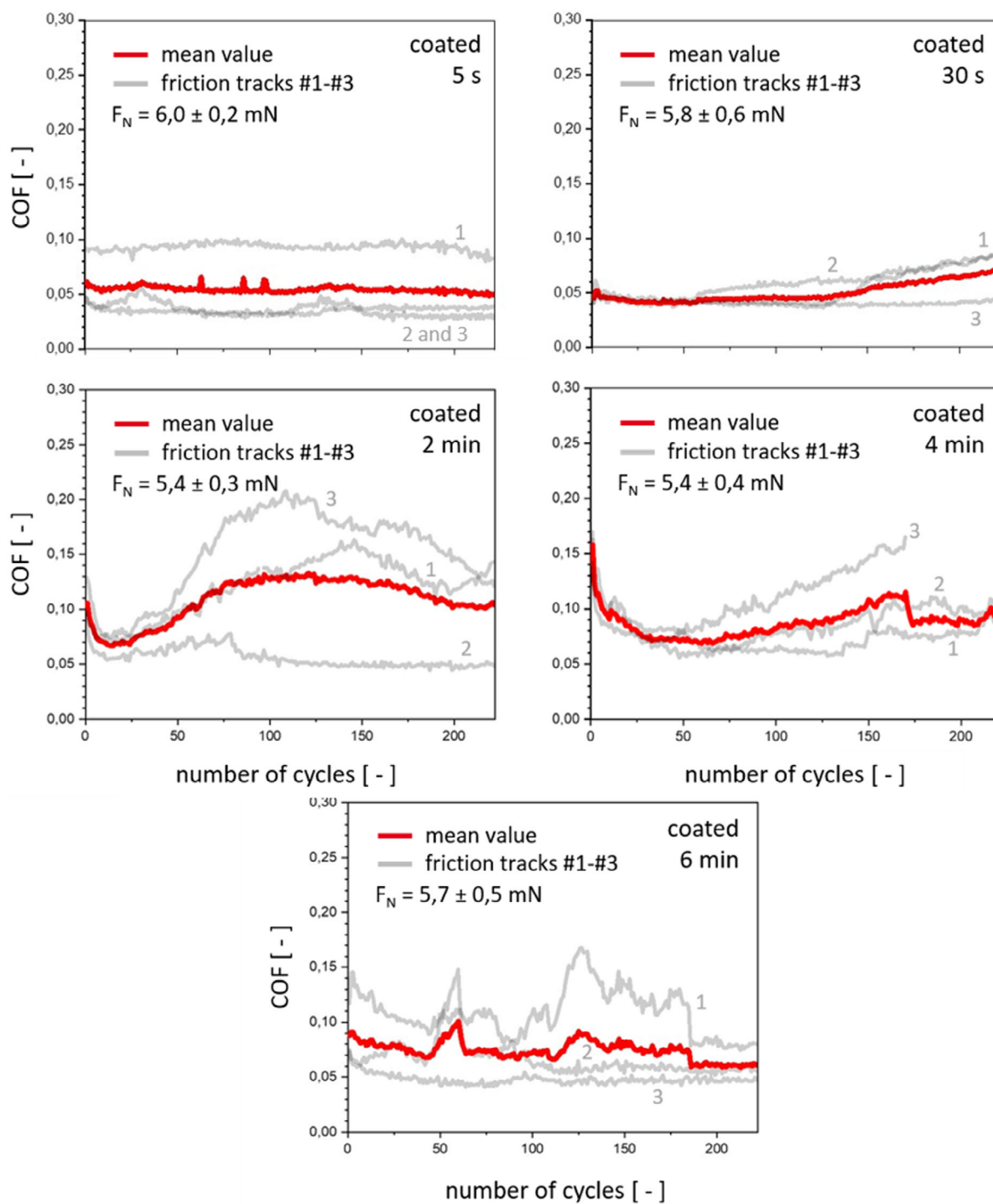


FIGURE 9 Coefficient of friction versus number of cycles for the UHV tribometer tests on the iron plates coated with friction modifier, gasization duration: 5 s, 30 s, 2 min, 4 min and 6 min, counterbody diamond sphere, nominal - normal force $F_N = 5$ mN (corresponding to a mean Hertzian pressure of 70 MPa), number of cycles $N = 222$, velocity $v = 50$ $\mu\text{m/s}$ (reverberating), grey curves: individual friction tracks (with indication of sequence), red curves: moving average of individual friction tracks.

(see Figure 7). To the best of our knowledge, this morphology has not been found previously in other gas phase lubrication studies to date (e.g. References [19,22–25]) using other friction modifier additives. In addition, the morphology is not consistent with the previously reported ‘thick film’ lubrication that has been seen in

interferometry studies.¹¹ In studies by Fry et al.,¹⁸ Benítez et al.¹⁷ and Zhu et al.,¹⁶ who also investigated the adsorption of amines on iron oxide or stainless steel surfaces, the authors assume layer formation.¹⁸

For the shortest deposition time, structures cannot be detected. After 30 s, the surface appears marbled in light

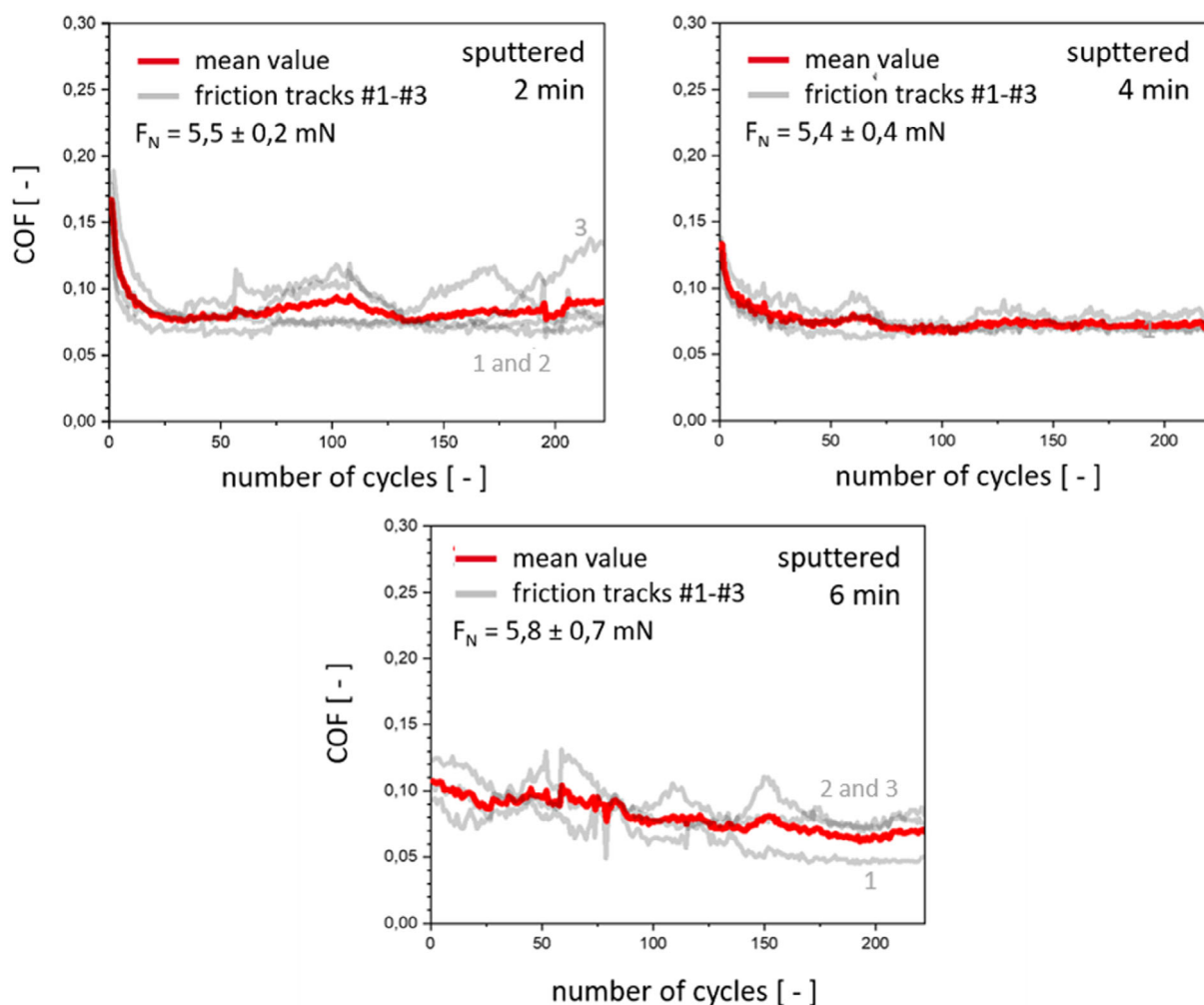


FIGURE 10 Coefficient of friction versus number of cycles for the UHV tribometer tests on the iron plates coated with friction modifier followed by sputtering, ablation <3 nm (friction traces in the sputter spot), vapour deposition duration: 2 min, 4 min and 6 min, counterbody diamond sphere, nominal - normal force $F_N = 5$ mN (corresponding to a mean Hertzian pressure of 70 MPa), number of cycles $N = 222$, velocity $v = 50$ $\mu\text{m/s}$ (reversing), grey curves: single friction marks (partially numbered), red curves: moving average of single friction marks.

microscopy images, and after 2 min, clearly punctiform structures can be recognised. An analysis of the droplet size showed radii of about 1 μm (graphically estimated) for 2 min, 3.2 ± 0.68 μm on average for 4 min and 3.5 ± 0.79 μm on averaged for 6 min. With the aid of automatic circle detection, a surface coverage of 27% (79 droplets per $[100 \times 100] \mu\text{m}^2$) was determined for the surface after 4 min of evaporation and a surface coverage of 26% (97 droplets per $[100 \times 100] \mu\text{m}^2$) after 6 min of evaporation. Strictly, it is not possible to discuss the influence of the layer thickness on the friction behaviour, but the influence of the droplet height and distribution. However, the droplet height cannot be precisely determined through the radius, since the droplets are so large that gravitational force has an influence.³⁰

For the deposition times of 2, 4 and 6 min, the surfaces covered with droplets were sputtered afterwards. Sputtering alters the droplet morphology so that a continuous film is formed on the surface. The detailed spectra of the XPS show no chemical changes due to this step. Only the very small measured intensity of the iron emission line indicates that a continuous additive film has formed. Assuming that this film is homogeneous, a film thickness d can be determined using formula (1):

$$d = \lambda_{\text{sub}} \cos \theta \ln \left(\frac{I_{\text{sub}}}{I_0} \right). \quad (1)$$

Here, I_0 describes the intensity of the elements initially present in the substrate, I_{sub} the intensity of the elements

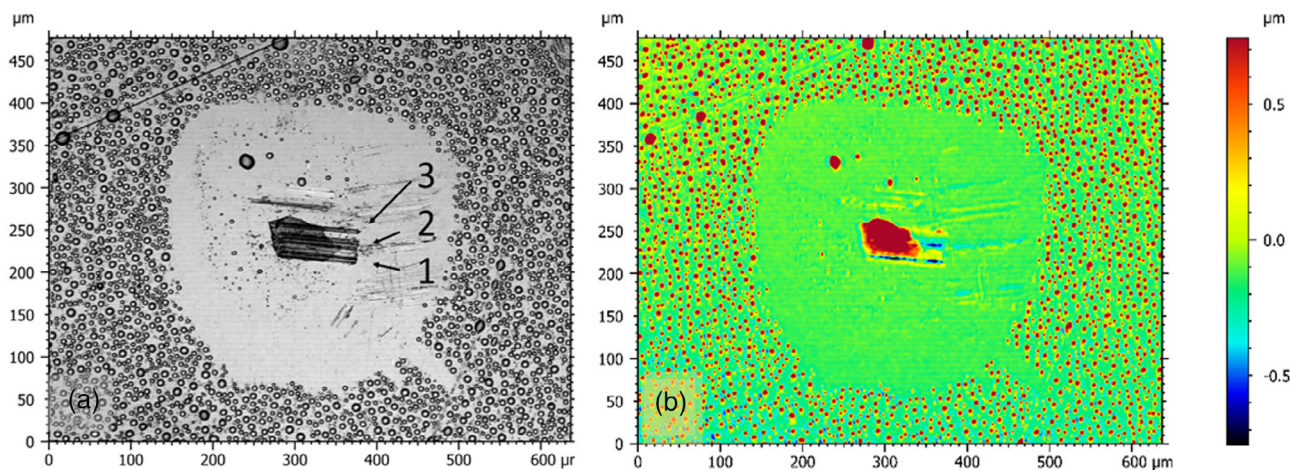


FIGURE 11 Grey image (a) and topography image (b) of the iron plate surfaces after the friction tests after 6 min of evaporation time with friction modifier (counterbody diamond sphere, nominal normal force $FN = 5$ mN [corresponding to a mean Hertzian pressure of 70 MPa], number of cycles $N = 222$, velocity $v = 50$ For Peer Review $\mu\text{m/s}$ [reversing]).

after coating, λ_{sub} the mean free path length in the substrate and θ the acceptance angle of the XPS, typically 45° . The film thicknesses determined in this way are 0.96 nm (2 min), 1.4 nm (4 min) and 1.55 nm (6 min) and thus become thicker with increasing evaporation times, corresponding to the larger and more numerous droplets.

In order to discuss the friction behaviour, it is necessary to point out an interesting phenomenon. In the image of the surface coated for 6 min and after the tribotest, a roughly circular, droplet-free area measuring approx. $350 \mu\text{m}$ in diameter can be seen (see Figure 11). Otherwise, an accumulation of liquid can be seen on the friction tracks. We ascribe this observation to capillary interactions that occurred between the diamond counterbody and the droplets. The evaluation of a force-time curve during the approach of the sphere to the coated surface shows an attractive interaction (supplementary information) and thus confirms the assumption. Unfortunately, the distance at which the attractive interaction begins, cannot be determined from the recorded curves. This information would give an indication of the actual droplet height. However, the real droplet height can be calculated with simple geometric considerations (see supplementary information):

$$h_{\text{real}} = r - \sqrt{r^2 - \left(\frac{d_{\text{real}} - s}{2}\right)^2}. \quad (2)$$

For an evaporation time of 6 min, formula (2) gives a real droplet height of $1.34 \mu\text{m}$. The ratio of height to radius for the friction modifier droplets in vacuum is

0.38. The droplet height after an evaporation time of 2 min is $0.38 \mu\text{m}$ and after 4 min $1.2 \mu\text{m}$.

Figure 12 shows the box plots of the friction coefficients for the tests on the coated iron plate surfaces after 5 s, 30 s, 2 min, 4 min, 6 min and for dry friction. Within the box are half of the measured values with the error bars indicating the standard deviation. In addition, the median line, the mean value and outliers are shown. The left side of Figure 12 shows the mean values of the friction coefficients over cycles 1–222 and this includes all ranges of the friction coefficient curves such as run-in, stabilisation phase and possible lubrication failure. Figure 12, right, shows the friction coefficient at the end of the friction test, for the 222nd cycle. The friction coefficient for dry friction, which summarises the results of dry friction test 1 and 2, is the highest, both for the mean value (0.244) and at the end (0.465). Dry friction test 3 on an iron plate with increased metallic iron content is not included in the calculation, as the surface is not comparable here. The smallest friction coefficients are found for the evaporation durations of 5 and 30 s. After 5 s, the mean value of the friction coefficient is 0.054 and at the end 0.05. After 30 s, the mean value of the friction coefficient is at the same level at 0.05 and at the end slightly higher at 0.074. The friction tests on the plates coated for 2 min have the highest friction coefficient both at the mean (0.109) and at the end (0.104). For the 4 and 6 min deposition durations, the coefficients of friction then decrease again to 0.088 and 0.074 on average and 0.093 and 0.061 at the end.

The trend within the tests with gas phase deposited friction modifier is explained on the basis of the droplet size and the associated capillary effect. Figure 13 shows

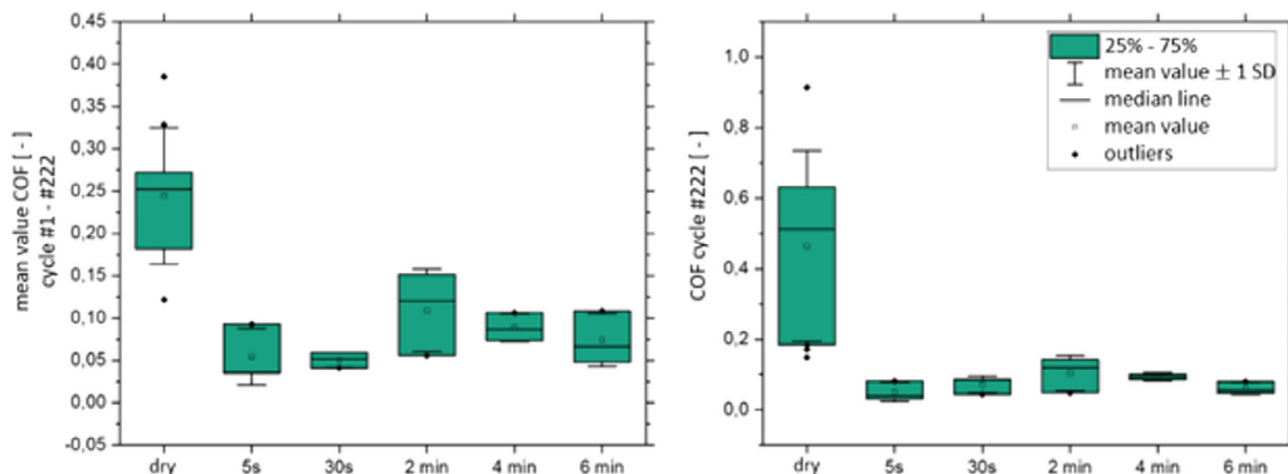


FIGURE 12 Boxplot of the friction values for the tests on the coated iron plate surfaces after 5 s, 30 s, 2 min, For Peer Review 4 min, 6 min and for dry friction (counterbody diamond ball, nominal normal force $F_N = 5$ mN, mean Hertzian pressure = 70 MPa), left: mean value of the friction coefficient over all cycles (1–222), right: friction coefficient at cycle 222. Half of the measured values lie within the box, the error bars indicate the standard deviation. In addition, the median line, the mean value and the outliers are shown.

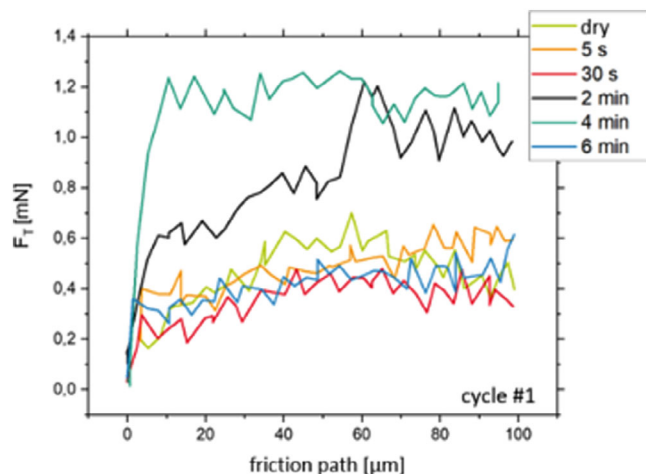


FIGURE 13 Friction force F_T over the friction path in cycle 1 for the experiments on the coated iron plate surfaces after 5 s, 30 s, 2 min, 4 min and 6 min and for the experiment dry friction 1 (counterbody diamond sphere, nominal normal force $F_N = 5$ mN, mean Hertzian pressure = 70 MPa)

the friction force curve over the friction distance (0–100 μm) of the first friction cycle. On these 100 μm , the droplets which have not already coalesced due to the approach of the diamond ball in the gap and form a large ‘droplet’ are collected. The friction forces for the dry test, as well as for the short evaporation durations of 5 and 30 s, are at a similar level around 0.4 mN. Interestingly, the curve of the experiment after 6 min of evaporation is also at this level. The tests after 2 and 4 min of evaporation both show a clear increase in the frictional force on the first 10 μm of the friction path, so that values of 1 and 1.15 mN are reached at the end of the path at 100 μm .

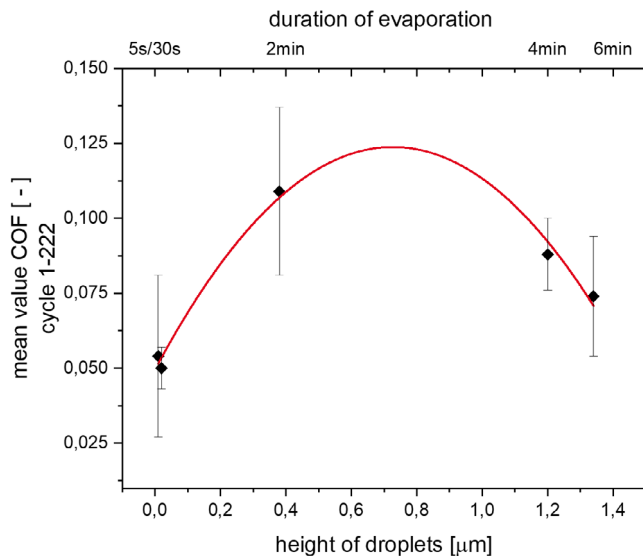


FIGURE 14 Mean value of friction coefficient over all cycles (1–222) versus droplet height of the gasized iron plates after 5 s, 30 s, 2 min, 4 min, and 6 min; red line corresponds to the parabolic fit function $f(x) = a + bx + cx^2$ with parameters $a = 0.05 \pm 0.004$, $b = 0.204 \pm 0.022$, and $c = 0.0163 \pm 0.016$ (R -squared = 0.97863, $N = 5$).

The additional frictional force that has to be applied here is attributed to the capillary forces acting. The diamond ball experiences not only the actual frictional force, but also the resistance due to the droplet and the associated force that must be applied to pull it along the friction gap. It can be assumed that after 6 min of evaporation, the droplet is so large and thus the volume of the friction gap is fully filled so that it no longer moves. This condition would correspond to friction in

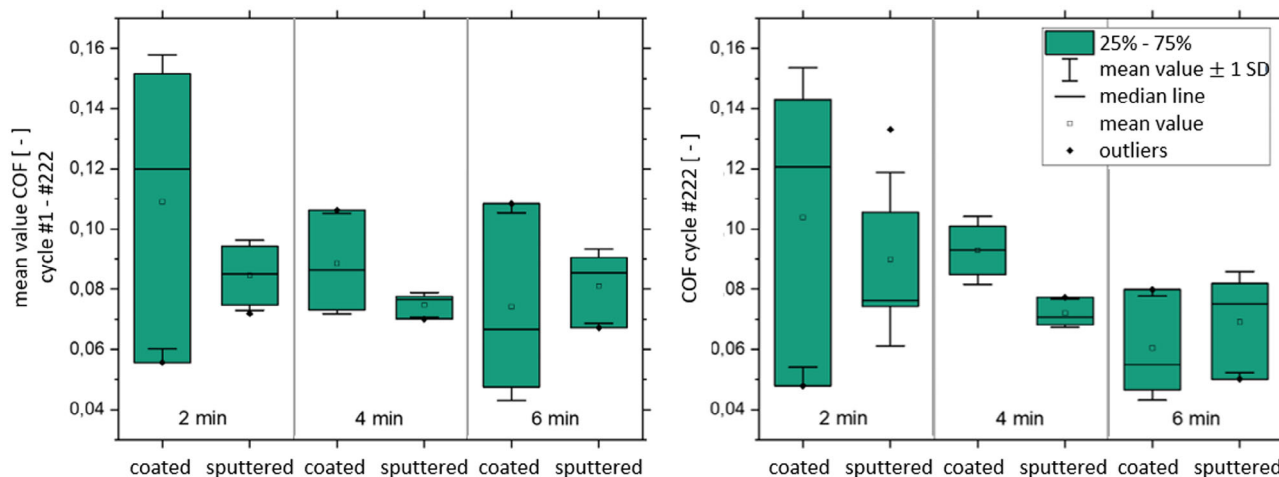


FIGURE 15 Boxplot of the friction values for the tests on the coated and afterwards sputtered iron plate For Peer Review surfaces after 2, 4, 6 min (counterbody diamond ball, nominal normal force $F_N = 5$ mN, mean Hertzian pressure = 70 MPa), left: mean value of the friction coefficient over all cycles (1–222), right: friction coefficient at cycle 222. Half of the measured values lie within the box, the error bars indicate the standard deviation. In addition, the median line, the mean value and the outliers are shown.

liquid. The additional force F_C to be applied can be determined from the difference between the friction force of the tests without capillary effect $F_{C,without}$ and with capillary effect $F_{C,with}$. For the levels of $F_{C,without}$ and $F_{C,with}$, values of 0.48 and 1.08 mN result, and thus a resulting capillary force F_K of 0.595 mN.

The plot of the mean friction coefficients versus droplet height (0.34 μm after 2 min, 1.2 μm after 4 min and 1.34 μm after 6 min) is shown in Figure 14. Considering the hypothesis that there is a critical droplet radius at which the friction coefficient starts to decrease again, a parabola can be fitted to the data (R -squared = 0.97863, $N = 5$). Very small values are assumed for the droplet heights after 5 and 30 s (0.01 and 0.02 μm). The critical droplet radius is thus 0.73 μm . Due to the limited data available, this value cannot be regarded as certain, but as plausible as a guide value. Since liquid friction can be assumed from an evaporation time of 6 min (possibly even earlier), the coefficient of friction should not decrease further for larger droplet radii.

If the surface covered with droplets is sputtered for a short time, a continuous layer of chemically unmodified friction modifier is formed. The layer thicknesses are 0.96 nm (2 min), 1.4 nm (4 min) and 1.55 nm (6 min). The decreasing trend for longer vapour deposition times can also be observed for the friction tests on the sputtered surfaces (see Figure 15). The highest mean and final friction values of 0.09 and 0.085, respectively, are found for the 2 min deposition and then sputtered surface. The friction value for the 4 min surface is 0.072 on average and 0.075 at the end. The measured coefficients of friction for the sputtered surfaces are lower than the corresponding coefficients of friction on the droplets as the capillary force is reduced. The coefficient of friction is higher after

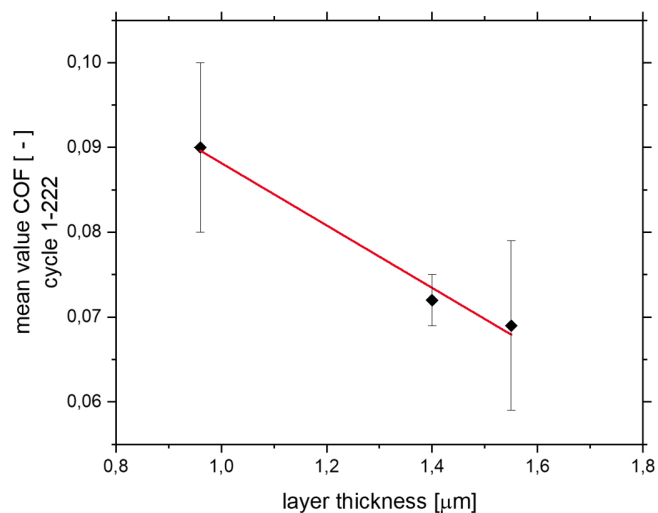


FIGURE 16 Mean value of the coefficient of friction over all cycles (1–222) versus layer thickness of the coated and afterwards sputtered iron plate surfaces after 2, 4, and 6 min; red line corresponds to the linear fit function $f(x) = a + bx$ with parameters $a = 0.125 \pm 0.006$ and $b = -0.037 \pm 0.004$ (Pearson- $R = -0.99344$, $N = 3$).

sputtering than on the droplets only for the 6 min coated sample, It is 0.069 on average and 0.081 at the end of the friction test. In addition, the trend shows that the scatter of friction values for the sputtered surfaces is smaller than for the friction values determined on the surfaces covered with droplets. This observation indicates that the scatter of the friction values on the droplets results from the fact that the small Hertzian contact area of approximately 0.007 mm^2 comes into contact with a different number of drops depending on the friction track (each measurement takes place at a new position). If the

friction value is plotted as a function of the coating thickness after sputtering, the coefficient follows a linear relationship (see Figure 16). Since we have observed that the droplets accumulate under the spherical counter surface, it is reasonable to speculate that the friction modifier will form similar thick films in lubricated contact when the additive is subjected to high shear. As a result the friction modifier loses the droplet-shaped morphology. The presented experimental strategy therefore allows systematic studies of the friction modifiers' film thickness without having to deal with hydrodynamic effects that change the lubricant film thickness.

6 | CONCLUSION

By using an effusion cell, a tribometer and an XPS in vacuum in tandem, it was possible to deposit a technical friction modifier on a defined iron oxide surface. This facilitated the study of the morphology as well as frictional behaviour of bespoke friction modifier without the influence of the base oil. In this environment, the additive forms droplets whose radii and heights increase with increasing deposition time. For 2 min deposition time the radius was about 1 μm . For 4 min (27% surface coverage) it was $3.2 \pm 0.68 \mu\text{m}$ on average, and $3.5 \pm 0.79 \mu\text{m}$ on average for 6 min (26% surface coverage). To the best of our knowledge, this morphology has not been found previously in other gas phase lubrication studies to date (e.g. References [19,22–25]) using other friction modifier additives. In friction tests, low friction values were observed for small (0.005) and large droplets (0.0074). In between, there are critical droplet sizes at which capillary effects occur and increase the coefficient of friction up to 0.109. This particular behaviour is expected of the correlation between droplet height and friction properties and should be further investigated with regard to the critical droplet height. For this purpose, tests with evaporation durations between 2 and 4 min are necessary. Furthermore, with durations >6 min, investigation as to whether the coefficient of friction decreases further or remains constant as assumed is reasonable. Subsequently, the findings obtained in vacuum are to be confirmed with experiments under lubricating conditions.

ACKNOWLEDGMENT

Open Access funding enabled and organized by Projekt DEAL.


CONFLICT OF INTEREST

The authors declare that they have no known competing financial interests or personal relationships that could have appeared to influence the work reported in this paper.

DATA AVAILABILITY STATEMENT

The data that support the findings of this study are openly available in Fordatis - Research Data Repository of Fraunhofer-Gesellschaft at <http://dx.doi.org/10.24406/fordatis/133>.

ORCID

Jennifer Eickworth  <https://orcid.org/0000-0003-3206-5872>

Martin Dienwiebel  <https://orcid.org/0000-0001-7682-0441>

REFERENCES

- Spikes H. Friction Modifier Additives. *Tribol Lett.* 2015;60(1): 119-145. doi:10.1007/s11249-015-0589-z
- Tang Z, Li S. A review of recent developments of friction modifiers for liquid lubricants (2007–present). *Curr Opin Solid State Mater Sci.* 2014;18(3):119-139. doi:10.1016/j.cossms.2014.02.002
- Bowden FP, Gregory JN, Tabor D. Lubrication of Metal Surfaces by Fatty Acids. *Nature.* 1945;156(3952):97-101. doi:10.1038/156097a0
- Daniel SG. The adsorption on metal surfaces of long chain polar compounds. *Trans Faraday Soc.* 1951;47:1345-1359. doi:10.1039/TF9514701345
- Loehle S, Matta C, Minfray C, et al. Mixed Lubrication with C18 Fatty Acids: effect of Unsaturation. *Tribol Lett.* 2014;53(1): 319-328. doi:10.1007/s11249-013-0270-3
- Campen S, Green JH, Lamb GD, Spikes HA. In Situ Study of Model Organic Friction Modifiers Using Liquid Cell AFM; Saturated and Mono-unsaturated Carboxylic Acids. *Tribol Lett.* 2015;57(2):51-71. doi:10.1007/s11249-015-0465-x
- Bernat S, Armada S, Espallargas. Friction Mechanisms by Carboxylic Acids in Aqueous Lubricants. *N. Tribol Lett.* 2018; 66(3):83. doi:10.1007/s11249-018-1035-9
- Kuwahara T, Romero PA, Makowski S, Weihnacht V, Moras G, Moseler M. Mechano-chemical decomposition of organic friction modifiers with multiple reactive centres induces superlubricity of ta-C. *Nat Commun.* 2019;10(1):151. doi:10.1038/s41467-018-08042-8
- Nehme GN, Dib M. Optimization of Mechanism of Boundary Lubrication in Fully Formulated Commercial Engine Oil Using Design of Experiment. *Tribol Trans.* 2011;54(2):208-226. doi:10.1080/10402004.2010.535192
- Hardy WB, Doubleday I. Boundary lubrication.— The paraffin series. *Proc R Soc A Math Phys Eng Sci.* 1922;100(707):550-574. doi:10.1098/rspa.1922.0017
- Anghel V, Bovington C, Spikes H-A. Thick-boundary-film formation by friction modifier additives. *Lubr Sci.* 1999;11(4):313-335. doi:10.1002/lvs.3010110402
- Ratoi M, Anghel V, Bovington C, Spikes H. Mechanisms of oiliness additives. *Tribol Int.* 2000;33(3–4):241-247. doi:10.1016/S0301-679X(00)00037-2
- Doig M, Camp PJ. The structures of hexadecylamine films adsorbed on iron-oxide surfaces in dodecane and hexadecane. *Phys Chem Chem Phys.* 2015;17(7):5248-5255. doi:10.1039/C4CP05837B
- Nalam PC, Pham A, Castillo RV, Espinosa-Marzal RM. Adsorption Behavior and Nanotribology of Amine-Based Friction

- Modifiers on Steel Surfaces. *J Phys Chem C*. 2019;123(22):13672-13680. doi:10.1021/acs.jpcc.9b02097
15. Wood MH, Welbourn RJL, Charlton T, Zarbakhsh A, Casford MT, Clarke SM. Hexadecylamine Adsorption at the Iron Oxide–Oil Interface. *Langmuir*. 2013;29(45):13735–13742. doi:10.1021/la4018147
 16. Zhu Y, Ohtani H, Greenfield M, Ruths M, Granick S. Modification of boundary lubrication by oil-soluble friction modifier additives. *Tribol Lett*. 2003;15(2):127-134. doi:10.1023/A:1024405115736
 17. Benítez JJ, Kopta S, Ogletree DF, Salmeron M. Preparation and Characterization of Self-Assembled Monolayers of Octadecylamine on Mica Using Hydrophobic Solvents. *Langmuir*. 2002;18(16):6096-6100. doi:10.1021/la011629y
 18. Fry BM, Moody G, Spikes HA, Wong JSS. Adsorption of Organic Friction Modifier Additives. *Langmuir*. 2020;36(5):1147-1155. doi:10.1021/acs.langmuir.9b03668
 19. de Barros Bouchet M-I, Martin J-M. Tribochemistry of n-Alkane Thiols Examined by Gas-Phase Lubrication (GPL). In: Dienwiebel M, de Barros Bouchet M-I, eds. *Advanced Analytical Methods in Tribology*. Springer International Publishing; 2018.
 20. Martin J-M, Le Mogne T, Grossiord C, Palermo T. Adsorption and friction in the UHV tribometer. *Tribol Lett*. 1997;3(1):87-94. doi:10.1023/A:1019183711497
 21. Marchetto D, Benzig R, Korres S, Dienwiebel M. Design and testing of ultrahigh vacuum microtribometer. *Tribol Mater Surf Interfaces*. 2012;6(3):95-101. doi:10.1179/1751584X12Y.0000000012
 22. Philippon D, de Barros-Bouchet M-I, Mogne TL, Gresser E, Martin J-M. Experimental simulation of phosphites additives tribochemical reactions by gas phase lubrication. *Tribol Mater Surf Interfaces*. 2007;1(3):113-123. doi:10.1179/175158408X273586
 23. Philippon D, de Barros-Bouchet M-I, Lerasle O, Le Mogne T, Martin J-M. Experimental Simulation of Tribochemical Reactions Between Borates Esters and Steel Surfaces. *Tribol Lett*. 2011;41(1):73-82. doi:10.1007/s11249-010-9685-2
 24. Philippon D, de Barros-Bouchet M-I, Le Mogne T, Lerasle O, Bouffet A, Martin J-M. Role of nascent metallic surfaces on the tribochemistry of phosphite lubricant additives. *Tribol Int*. 2011;44(6):684-691. doi:10.1016/j.triboint.2009.12.014
 25. Righi MC, Loehlé S, de Barros Bouchet M-I, Philippon D, Martin J-M. Trimethyl-phosphite dissociative adsorption on iron by combined first-principle calculations and XPS experiments. *RSC Adv*. 2015;5(122):101162-101168. doi:10.1039/C5RA14446A
 26. Rana R, Tysoe W. Tribochemical Mechanisms of Trimethyl and Triethyl Phosphite on Oxidized Iron in Ultrahigh Vacuum. *Tribol Lett*. 2019;67(3):93. doi:10.1007/s11249-019-1205-4
 27. Martin J, Le Mogne T, Boehm M, Grossiord C. Tribochemistry in the analytical UHV tribometer. *Tribol Int*. 1999;32(11):617-626. doi:10.1016/S0301-679X(99)00090-0
 28. Jung AK, Voelkel L, Crema S. Composition and method to improve the fuel economy of hydrocarbon fueled internal combustion engines. EP 2321389B1.
 29. Eickworth J, Wagner J, Daum P, Dienwiebel M, Rühle T. Raw Data: Gas phase lubrication study with an organic friction modifier. doi:10.24406/fordatis/133
 30. Mugele F, Heikenfeld J. *Electrowetting*. John Wiley & Sons, Ltd; 2018.

SUPPORTING INFORMATION

Additional supporting information can be found online in the Supporting Information section at the end of this article.

How to cite this article: Eickworth J, Wagner J, Daum P, Dienwiebel M, Rühle T. Gas phase lubrication study with an organic friction modifier. *Lubrication Science*. 2022;1-16. doi:10.1002/ls.1620